International Journal of Technology 15(4) 952-964 (2024)
Received June 2022 / Revised August 2022 / Accepted February 2023

International Journal of Technology

http://ijtech.eng.ui.ac.id

Polypropylene-based Bio-nano Composites Reinforced with Cellulose Nanocrystals and Added with Mono-diacylglycerols as Antistatic Agent

Dwi Setyaningsih[1,2,*], Muhammad Syukur Sarfat[1], Farah Fahma[1], Nastiti Siswi Indrasti[1]

[1]*Department of Agroindustrial Technology, IPB University, Bogor 16680, West Java, Indonesia*
[2]*Surfactant and Bioenergy Research Center, IPB University, Bogor 16144, West Java, Indonesia*

Abstract. This research aims to identify the performance and mechanical characteristics of polypropylene-based antistatic bio-nano composites reinforced with 2% mono-diacylglycerols (M-DAG) and 0, 0.5, 2.5% cellulose nanocrystals (CNC) and compared to pure PP. Based on the results of SEM on cross-section, there was an agglomeration of M-DAG and CNC on the PP matrix. XRD diffractogram pattern of antistatic bio-nano composites showed peaks representing the diffraction structure of glycerol monostearate and cellulose I. The FTIR spectrum of each formulation was very similar to the characteristic peaks of PP and showed three distinct peaks compared to pure PP. The melting temperature of antistatic composites without CNC (176.54 ^{0}C) was higher than pure PP (175.44 ^{0}C). Thermal stability of antistatic bio-nano composites with 0, 0.5, and 2.5% CNC were 472.07, 470.25, and 475.15 ^{0}C, respectively, higher than pure PP (468.27 ^{0}C). The best mechanical properties were 2.5% CNC with 11.071 MPa flexural modulus, 30.376 MPa tensile strength, 23.796% tensile elongation, 1.659 J/m^2 impact strength, which were higher than pure PP, and it generated antistatic activity of 10^{10} - 10^{12} Ω/sq resistivity.

Keywords: Antistatic bio-nano composites; Biopolymers synthesis; Cellulose nanocrystals; Mono-diacylglycerols; Polypropylene

1. Introduction

The trend of using synthetic polymer-based materials is predicted to increase in terms of fulfilling human needs. Synthetic polypropylene (PP) is known for having a high softening point or glass transition, high resistance to bending stress, low water absorption, good electrical resistance, light dimensional stability, high impact strength, non-toxicity properties, and the degree of crystallinity ranges from 40 to 60% with the melting temperature range from 130 to 171°C (Shubhra, Alam, and Quaiyyum, 2013). But PP is susceptible to high temperatures, flammable, prone to UV degradation, susceptible to oxidation, difficult to paint, and harmful to the environment due to its non-degradable nature (Purnomo, Baskoro, and Muslim, 2021; Shieddieque *et al.*, 2021), but PP is recyclable (Jain and Tiwari, 2015). Therefore, to overcome the weakness, it is necessary to modify PP into bio-nano composites. Antistatic bio-nano composites are synthesized by adding natural antistatic materials.

Nanocomposites are multicomponent materials consisting of several different phases in which at least one phase size is in the nanoscale (less than 100 nm) (Sandri *et al.*, 2016).

*Corresponding author's email: dwisetyaningsih@apps.ipb.ac.id, Tel.: +628158314669
doi: 10.14716/ijtech.v15i4.5746

The antistatic bio-nano composites synthesized using mono-diacylglycerols (M-DAG) as an antistatic agent (Salsabila *et al.,* 2021), cellulose nanocrystals (CNC) as a reinforcement, and PP as a thermoplastic matrix (Clemons and Rick, 2020; Sabaruddin, Md-Tahir, and Lee, 2019; Gwon *et al.*, 2018). A combination of M-DAG and CNC is expected to produce a synergistic effect to improve the quality of the antistatic bio-nano composites. The addition of M-DAG and CNC to the PP matrix had a positive impact on the characteristics of the resulting bio-nano composites and antistatic bio-nano composites (Sabaruddin, Md-Tahir, and Lee, 2019; Gwon *et al.*, 2018).

M-DAG is an ester of glycerol and free fatty acid (FFA) which has unreacted or free hydroxyl groups. MAG, or monoglyceride, has a single fatty acyl chain, while DAG, or diacylglyceride, has two fatty acyl chains (Sarfat *et al.*, 2022). This free hydroxyl group makes M-DAG a non-ionic surfactant that is degradable and bio-compatible, so it is widely used in the food, cosmetic, and pharmaceutical industries. This free hydroxyl group allows M-DAG to be used as a stabilizer and an antistatic agent in bio composites or plastics (Salsabila *et al.*, 2021). M-DAG used in this research was produced from palm fatty acid distillates (PFAD) from the refining process of crude palm oil (CPO) (Setyaningsih, Suwarna, and Muna, 2020; Setyaningsih *et al.*, 2020).

CNC is a cellulose-based nanomaterial that has better mechanical characteristics such as tensile strength (7.5 GPa) (Tang *et al.*, 2017), tensile modulus (100 - 140 GPa) (Tang *et al.*, 2017), high surface area (569 m^2/g) (Brinkmann *et al.*, 2016), with a diameter average of 8 nm (Rochardjo *et al.*, 2021) compared to other cellulose-based nanomaterials such as cellulose nanofiber (CNF) which has a tensile strength of 0.3833 GPa (Kafy *et al.*, 2017), a tensile modulus of 23.9 GPa (Kafy *et al.*, 2017) and surface area of 430 m^2/g (Moser, Henriksson, and Lindström, 2016). However, there are disadvantages of CNC, namely low stability starting from 283.55 ^{0}C, which causes CNC to be very susceptible to high heat treatment when used as a reinforcing material in polymer matrices. M-DAG can be used as a lubricant and stabilizer to protect CNC from thermal degradation during processing.

Therefore, a combination of M-DAG and CNC as additive materials for the synthesis of PP-based antistatic bio-nano composites has a prospect as next-generation material that is more flexible in use and exhibits superior performance and mechanical characteristics compared to pure PP. There has never been researched that combines M-DAG and CNC simultaneously as reinforcement in the PP matrix. Therefore, this study aims to evaluate the performance and mechanical characteristics of PP-based antistatic bio-nano composites reinforced with varying concentrations of M-DAG and CNC, and compare them to those of pure PP.

2. Methods

2.1. Raw Materials

The raw materials for synthesizing antistatic bio-nano composites were PP, M-DAG, and CNC. PP (PT Chandra Asri Petrochemical Tbk) has a melt flow index of 10 g/10 minute and a density of 0.903 g/cm^3. M-DAG (SBRC-LPPM-IPB) has a crystallinity index of 92.85%, a diameter of 0.11–1.78 nm, and a thermal degradation rate of 200.50 ^{o}C. CNC (CelluForce Co.) has a density of 1.5 g/cm^3, a crystallinity index of 98.95%, and diameter of 3.39–12.72 nm, a length of 44 – 108 nm, and thermal degradation of 296.96 ^{o}C. The supporting materials consist of maleic anhydride polypropylene (MAPP)(BYK Chemie GmbH), antioxidant (AO) (BASF Schweiz AG, Switzerland), and mineral oil (MO) (Arkema France).

2.2. Methodology

The synthesis of antistatic bio-nano composites involved six stages: mixing, extruding, master batching, drying, pelletizing, and molding (as shown in Figure 1). The mixture comprised 77.88% PP, 15% CNC, 5% M-DAG, 2% MAPP, 0.1% AO, and 0.02% MO, and was extruded using a twin-screw extruder at a temperature range of 180–220 ^{0}C and a screw speed of 150 rpm. This process resulted in the production of pellets masterbatch. The formulation of main raw materials (M-DAG and CNC) for synthesizing antistatic bio-nano composites, which entered the masterbatch process, was determined based on literature studies and trial and error. The formulation of supporting materials (MAPP, AO, and MO) was determined based on the standard use in Technical Data Sheet (TDS). The mixture of PP, CNC, M-DAG, and masterbatch pellets was injected using an injection molding machine at a temperature of 180–220 ^{0}C to produce antistatic bio-nano composites plates (5 x 8 cm^2) at a concentration of 0, 0.5, 2.5% CNC and 2% M- DAG. The plates were then cooled to room temperature of 25 ^{0}C, 3 MPa pressure for ±24 hours at 50% humidity before characterization. Table 1 shows the composition of each treatment.

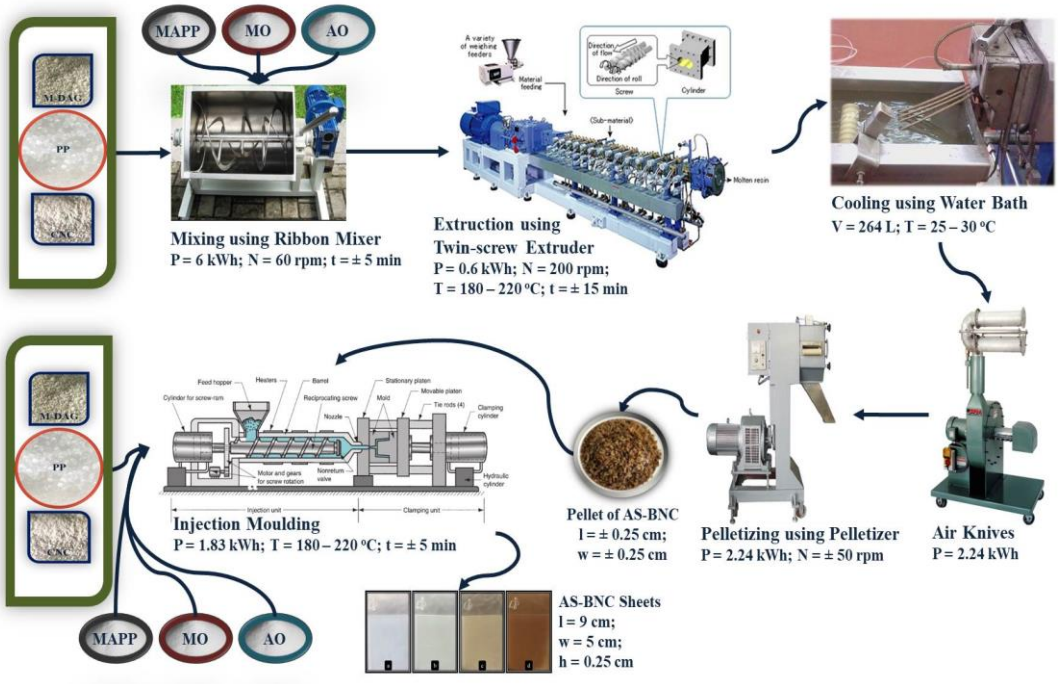

Figure 1 The Stages of the synthesis of antistatic bio-nano composites

Table 1 Formulation of antistatic bio-nanocomposites

	Concentration (%)					
Treatment	PP	M-DAG	CNC	MAPP	MO	AO
Pure PP	99.88	0	0	0	0.02	0.1
AS-BNC-0	97.88	2	0	0	0.02	0.1
AS-BNC-0.5	95.38	2	0.5	2	0.02	0.1
AS-BNC-2.5	93.38	2	2.5	2	0.02	0.1

Note: AS-BNC: antistatic bio-nano composites

2.2. Antistatic Bio-nano Composites Characterization

Morphological analysis used scanning electron microscopy (SEM). The SEM used was JEOL Standard on JSM-6510LA (electrical image shift ± 5 µm and ± 10 µm (WD = 10 mm), resolution mode 10 kV and 20 kV). Degree of crystallinity analysis used X-ray diffraction (XRD), Labx - XDR 600 equipment from Shimadzu with Cu-Kα radiation (λ = 1.5406 Å), 2θ

in the range between 0° to 80°, rate scanning of 2°/min and the total exposure time of 40 min. To identify crystal peaks, degree of crystallinity, and amorphous composition, we used Mach! Version 3.11.3.192 and the Crystallography Open Database (COD) inorganic reference database. The crystal size τ (nm) perpendicular to the lattice plane (002) of cellulose was determined using the Scherrer equation (Saleh, 2021), as calculated in Equation 1.

$$\tau = \frac{K\lambda}{\beta_{hkl}\cos\theta} \quad (1)$$

where τ is the crystal size in the perpendicular direction of the hkl lattice plane, K is the Scherrer constant (0.94), λ is the X-ray wavelength (1.54 A°), β is the full width at having the greatest according to the hkl peak in radians, and θ is the angle Bragg.

Infrared spectrum analyzed using Fourier transform IR (FT-IR) Thermo Fisher Scientific Nicolet iS5 spectrophotometer with cleaning pump and wavelengths 300 cm^{-1} to 4000 cm^{-1}, 128 accumulated scans, resolution 4 cm^{-1}, in ATR and transmittance module. Thermal properties analysis used differential scanning calorimetry (DSC) TA Instruments, New Castle, UK model Q200. Dynamic DSC scans were conducted in the temperature range from 23 to 400 °C at a heating rate of 10 °C/min. The crystallization and melting behaviors were recorded in a nitrogen atmosphere, at the range mass used of 21.8 to 29.0 mg.

Analysis of tensile properties (ASTM D-638) included tensile modulus, tensile strength, maximum tensile strength, tensile elongation, and elongation at break. Specimens were prepared by compression molding. Dumbbell specimens were cut from compression-molded sheets with a thickness of 3.2 mm. The tensile test was carried out at a crosshead speed of 2.8 mm/min, and a pre-load of 0.25 N. Tensile properties for each treatment were evaluated from the stress-strain data. Impact strength analysis used the ASTM D-256 method. The standard specimen was 64 mm long, 12.7 mm wide, and 6 mm thick. Impact strength Is (J/m2), calculated using Equation 2 (McKeen, 2014).

$$I_s = \frac{W}{hb}10^{-3} \quad (2)$$

where W is the corrected energy absorbed by breaking the specimen (J), h is the thickness of the specimen (mm), and b is the width of the specimen (mm).

The analysis of flexural properties consists of flexural strength (Equation 3) and flexural modulus (Equation 4) (Chakraborty and Ratna, 2020; Bhatnagar and Asija, 2016).

$$\mathcal{S} = \frac{3Ps}{4wh^2}\left[1 + 6\left(\frac{\delta}{s}\right)^2 - 4\left(\frac{\delta h}{s^2}\right)\right] \quad (3)$$

$$E_s = \frac{Ps^3}{4w\delta h^3} \quad (4)$$

where S is flexure strength (N/mm2/MPa), E_s is flexure modulus (N/mm2/MPa), P is breaking load (N), s is support span (mm), w is beam width (mm), h is the thickness of the beam (mm), and δ is the deflection at the center of the span (mm).

The surface resistivity (ASTM D257-99) used Advantest R8340 Ultra High Resistance Meter. The surface resistivity (before and after exposure to room temperature for 1 – 7 weeks) was determined using Equation 5 (Maryniak, Uehara, and Noras, 2003). The thickness of the specimen, test voltage, and test time were 1 mm, 500 V, and 1 minute, respectively.

$$\rho_s = \frac{2\pi}{\ln\left(\frac{R_2}{R_1}\right)}R_s \quad (5)$$

where ρ_s is the surface resistivity (Ω/sq), R_s is the surface resistance (ohms), π is the ratio of the circumference of a circle to its diameter equal to 3.14, R_1 is the outer radius of the center electrode (cm), R_2 is the inner radius of the outer ring electrode (cm).

3. Results and Discussion

3.1. Morphology Analysis

SEM was carried out for morphological inspection of the antistatic bio-nano composites (AS-BNC) cross-section at 500, 1000, 2500, and 5000x magnification (Figure 2).

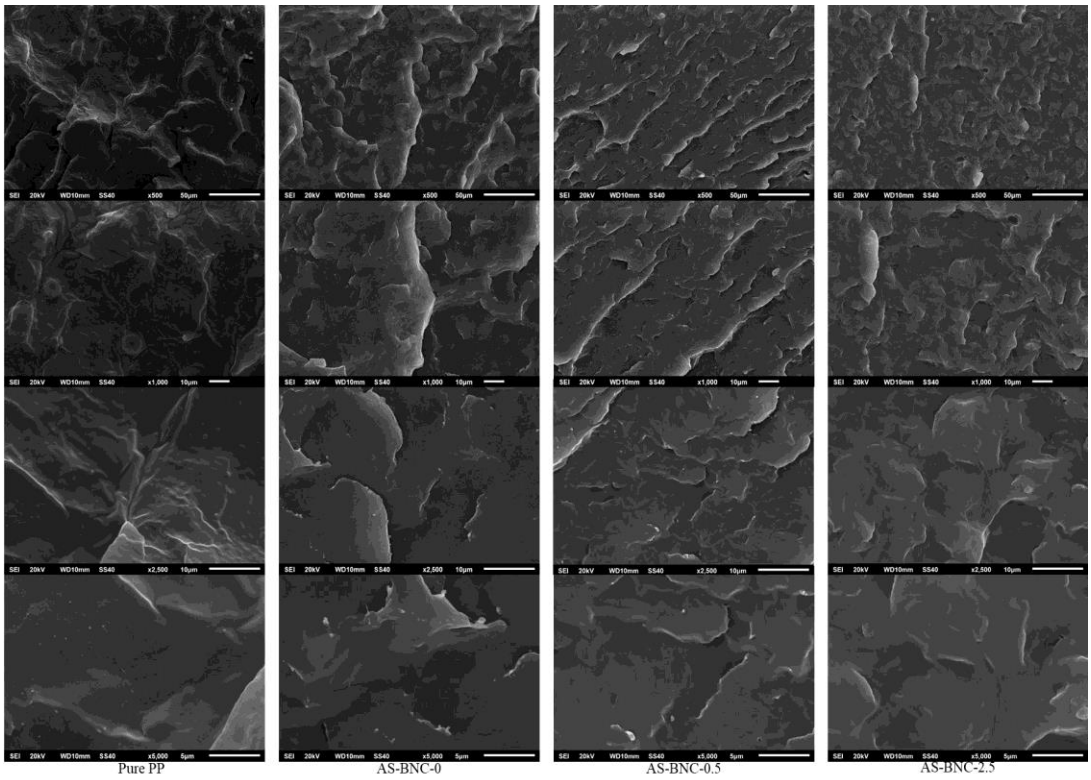

Figure 2 Morphological analysis of antistatic bio-nano composites using SEM

Based on the results of the SEM analysis on the cross-section, M-DAG agglomeration was found on the PP matrix because it shows a morphological form of M-DAG, while the CNC is not visible. This indicates a chemical reaction or physical interaction between M-DAG and the PP matrix. Physical interaction occurs when the polar groups (palmitate) are oriented to the PP matrix. In contrast, the polar groups (glyceryl) are oriented away from the PP matrix towards the antistatic bio-nano composite surface, and it is possible to interact physically with CNC. Another possibility is that the polar group (glyceryl) reacts with the O group of the maleic anhydride during the synthesis process. In addition, there was no fibrillation on the surface of the antistatic bio-nano composites cross-section. This implies that no significant plastic deformation occurred in the antistatic bio-nano composites layer during fracture, although the CNC concentration is increased. According to Shojaeiarani, Bajwa, and Chanda (2021), the rheological properties of CNC-filled polymer melts depend on factors such as the degree of CNC particle dispersion, their orientation state, and aspect ratio. Consequently, the rheological properties of the antistatic bio-nano composites in our study were also influenced by these factors. In particular, the homogeneous dispersion of CNC particles led to more effective load transfer to the reinforcements.

3.2. Degree of Crystallinity and Particle Size Analysis

Crystallinity analysis was carried out on AS-BNC using XRD analysis to observe changes in the crystal structure as a function of chemical treatment and to measure the degree of crystallinity (CrI) using the deconvolution method with a ratio between the area corresponding to the crystal peak and the total area (Park *et al.*, 2010). Figure 3A shows the XRD diffractogram of AS-BNC. XRD diffractogram patterns were recorded using Cu K irradiation, λ = 1.5418 A.

The results of the XRD diffractogram analysis of AS-BNC showed with seven peaks with peak heights ranging from 87.09 – 1000 I rel of AS-BNC-5, 84.61 – 1000 I rel of AS-BNC-0.5, and 90.91 – 1000 I rel of AS-BNC-2.5 (Table 2). The XRD diffractogram pattern showed peaks representing the diffraction structure of glycerol monostearate and cellulose I. The diffraction characteristic of glycerol monostearate can be observed in the peak range between 5^0 to 30^0 (Yusuf *et al.*, 2013). The diffraction characteristics of cellulose I could be observed around peaks at 15^0 (001), 22.5^0 (002), and 34^0 (040) (Park *et al.*, 2010), Couret *et al.* (2017) said the peaks at 15^0 (1-10), 17^0 (110), 21^0 (102/012), 23^0 (200), and 34^0 (004) represent the diffraction structure of cellulose I.

The XRD diffractogram of PP showed the pattern, which has seven peaks with peak heights ranging from 85.41 – 1000 I rel. According to Guerra, Wan, and McNally (2019), the XRD patterns showed the most intense peaks for PP at 2θ = 16.5^0 α(100), 19.2^0 β(300), 20^0 α(040), 22^0 α(130), and for the GNPs at 2θ = 32^0 (002).

Table 2 Particle size, degree of crystallinity, and percentage of amorphous components

Treatments	Diffractogram pattern (2θ [^{0}])	Peak heights ranging (I rel)	Average particle size (nm)	Degree of crystallinity (%)	Amorphous components (%)
Pure PP	13.97 – 25.34 (16.80)*	85.41 – 1000	15.52	90.54	9.46
AS-BNC-0	13.99 – 25.39 (16.83)*	87.09 – 1000	15.84	89.97	10.03
AS-BNC-0.5	13.97 – 25.36 (16.80)*	84.61 – 1000	15.85	89.81	10.19
AS-BNC-2.5	13.99 – 25.36 (16.80)*	90.91 – 1000	16.01	91.10	8.90

Note: * The diffractogram pattern of the highest peak

The identification results of the particle size, degree of crystallinity, and percent of amorphous components in AS-BNC showed the average particle sizes between 15.84 to 16.01 nm, 89.81 to 91.10 % degree of crystallinity, and 8.90 to 10.19 % amorphous components (Table 2). The particle size of AS-BNC was increased with the increase in CNC concentration. The degree of crystallinity of AS-BNC-2.5 is higher than that of pure PP.

3.3. Infrared Spectrum Analysis

The FTIR spectrum of each treatment (Figure 3B) was very similar to the characteristic peaks of PP and depicted distinct tri peaks for the antistatic bio-nano composites compared to the pure PP. The first distinct absorption peak ranging from 1200 cm^{-1} to 1000 cm^{-1} were primarily assigned to C–O–C bond, C–C bending, and ring structures (with typical sharpening at 1071.50 cm^{-1} with %T of 85.14% and 1166.98 cm^{-1} with %T of 69.93% (AS-BNC-0), 1080.18 cm^{-1} with %T of 83.03% and 1166.02 cm^{-1} with %T of 64.77% (AS-BNC-0.5), and 1085.01 cm^{-1} with %T of 74.86% and 1166.02 cm^{-1} with %T of 51.02% (AS-BNC-2.5), which correspond to typical cellulose and glycerol compound (Al-Haik *et al.*, 2020). In the band around 1080 cm^{-1}, the %T decreased as the concentration of CNC added to the PP matrix increased, while the %T in Pure PP was lower than each of the AS-BNC, which was 70.79%. This indicated the presence of an increasing C–O–C bond due to ring deformation of maleic acid compounds or ring widening and C–O stretching. The same phenomenon occurred in the band around 1166 $cm^{-1,}$ which showed a decrease of %T with increasing

concentration of CNC addition to the PP matrix, but lower than Pure PP (68.11%), except for AS-BNC-0. This indicated the presence of an increasing C–C bending.

The second distinct band is related to the wavelength near 2900 cm^{-1}. This broadband was assigned to stretching vibration of C–H hydroxyl groups asymmetric stretching of cellulose and glycerol. In this band, % transmittance (T) decreased as the concentration of CNC increased, while %T in pure PP was higher than AS-BNC. The presence of these bands confirmed the interaction of CNC and the distribution of M-DAG in the PP matrix. Due to this interfacial adhesion, the overall mechanical properties were enhanced for the AS-BNC. Hobuss *et al.* (2020) determined the asymmetric and symmetric C–H stretching mode of the fatty acid chain methylene group at 2922 cm^{-1} and 2853 cm^{-1}. The third distinct peak was 3315 $cm^{-1,}$ which is related to O–H [ν (O–H)] stretching, a characteristic of hydroxyl groups. This band showed that %T decreased as the concentration of CNC increased, while %T of pure PP was higher than AS-BNC. Hobuss *et al.* (2020) set the O–H stretch at 3360 cm^{-1}.

The bands at 1377.23 cm^{-1} and 1457.28 cm^{-1} in all treatments were characteristics of PP (Fang *et al.*, 2012). The absorption bands at 1738.90 cm^{-1} (Pure PP), 1742.76 cm^{-1} (AS-BNC-0), 1738.90 cm^{-1} (AS-BNC-0.5), and 1742.76 cm^{-1} (AS-BNC-2.5) were observed, which were assigned to the absorption of carbonyl groups (C=O) of maleic anhydride (MA) (Rahman, Hassan, and Heidarian, 2018; Zhou *et al.*, 2013). Finally, the spectrum on the peak 1166.02 cm^{-1} indicated the C-C bending, which was the backbone of PP (Fang *et al.*, 2012).

The infrared (IR) spectrum of the antistatic bio-nano composites revealed several characteristic peaks. Specifically, peaks between 3300 cm^{-1} and 3250 cm^{-1} were assigned to O–H stretching modes, while those between 3000 cm^{-1} and 2750 cm^{-1} corresponded to the stretching modes of CH, CH_2, and CH_3 groups. The peak at 1750 cm^{-1} was indicative of carbonyl stretching (C = O). The peaks between 1500 cm^{-1} to 1250 cm^{-1} were characteristic of the deformation of the CH_2 and CH_3 groups. The peaks between 1250 cm^{-1} to 1150 cm^{-1} were referred as the C–O and C–C bonds. The peak at 1100 cm^{-1} was also characteristic of the strain of the C–O bond and ester group (–C–O–C–). The "wag" vibration and asymmetric angular deformation of CH and CH_2 groups were found at 750 cm^{-1} (Hobuss *et al.*, 2020).

3.4. Thermal Properties and Melt Flow Index Analysis

Based on the identification results of the thermal properties (Figure 3C and Table 3), it was found that the melting temperature of AS-BNC-0 was 176.54 ^{0}C higher than that of pure PP 175.44 ^{0}C. The melting temperature of AS-BNC-0.5 and AS-BNC-2.5 were 171.70 ^{0}C and 174.38 ^{0}C, respectively, slightly lower than that of pure PP. However, when compared between AS-BNC-0.5 and AS-BNC-2.5, AS-BNC-2.5 had a higher melting temperature than AS-BNC-0.5. This indicated an opportunity for increasing melting temperature with an increase in CNC concentration. According to Al-Haik *et al.* (2020) and Hejna *et al.* (2017), the melting temperature of bio-nano composites with the addition of 2%, 4%, and 5% CNC on the PP matrix showed a higher value when compared to pure PP and the addition of 4% CNC had the higher melting temperature than 3% CNC. According to Yousefian and Rodrigue (2016), the distribution of CNC particles in the polymer matrix greatly influenced the thermal properties of the resulting bio-nano composites.

Thermal stability of AS-BNC-0, AS-BNC-0.5, and AS-BNC-2.5 was 472.07 ^{0}C, 470.25 ^{0}C, 475.15 ^{0}C respectively, higher than pure PP (468.27 ^{0}C). Therefore, the addition of 2.5% CNC and 2% M-DAG to the PP matrix can increase the thermal degradation of the resulting antistatic bio-nano composites. The higher the degree of crystallinity of the antistatic bio-nano composites, the higher the thermal stability, except for the antistatic bio-nano composites treated with AS-BNC-0. According to Al-Haik *et al.* (2020), the thermal stability of bio-nano composites with the addition of 1%, 2%, and 3 % CNC on the PP matrix showed

a higher value when compared to pure PP and the addition of 4% and 5 % CNC. It showed that the addition of 3 % CNC has the highest thermal stability. CNC particles were thought to increase the thermal resistance of AS-BNC by inhibiting the diffusion of volatile decomposition products or by forming a charred CNC surface that dissipates heat by absorbing it in the inorganic phase (Thomas *et al.*, 2018; Ng *et al.*, 2017). In addition, the presence of M-DAG can inhibit the thermal degradation of AS-BNC. The reduced thermal resistance in AS-BNC with 2% M-DAG and 0.5% CNC may have been due to the non-uniform dispersion of the CNC particles (Ng *et al.*, 2017).

Table 3 Thermal properties of antistatic bio-nano composites

Parameters	Antistatic bio-nano composites			
	Pure PP	AS-BNC-0	AS-BNC-0.5	AS-BNC-2.5
T_m (^{0}C)	175.44	176.54	171.70	174.38
T_g (^{0}C)	468.27	472.07	470.25	475.15
ΔH_m (J/g)	111.75	102.66	87.62	123.72
Peak height (mW)	-16.44	-30.44	-21.72	-20.88
T_{onset} (^{0}C)	125.79	158.32	150.79	123.53
T_{offset} (^{0}C)	228.24	196.26	196.16	227.40
Baseline type	Linear	Linear	Linear	Linear

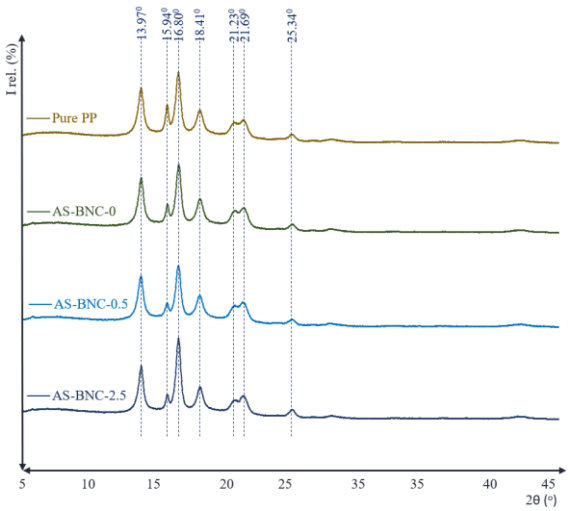

A. XRD diffractogram

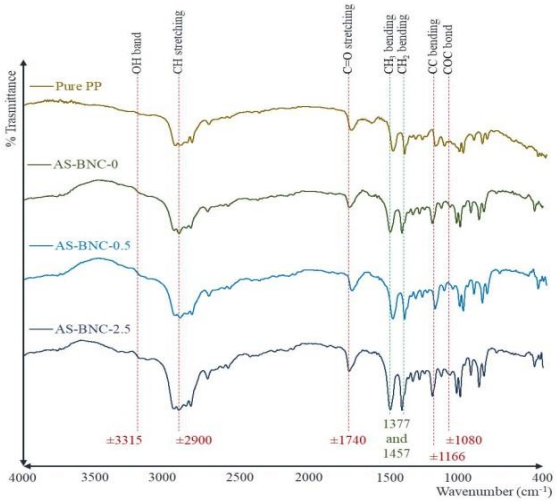

B. IR Spectra

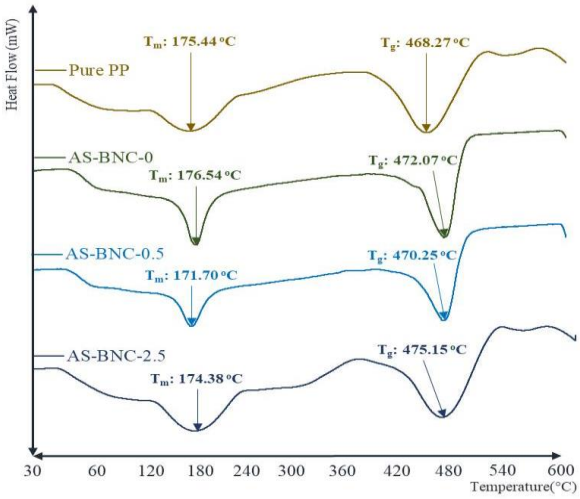

C. DSC thermogram

Figure 3 XRD diffractogram (A), FT-IR spectra (B), and DSC thermogram of AS-BNC

3.5. Mechanical Properties Analysis

Analysis of mechanical properties of AS-BNC includes tensile properties (Table 4) and flexural, impact strength, and surface resistivity properties (Table 5). The best AS-BNC was AS-BNC-2.5 with 11.071 MPa flexural modulus, 30.376 MPa tensile strength, 23.796% tensile elongation, 1.659 J/m^2 impact strength, and 10^{10} – 10^{12} Ω/sq resistivity, which was higher than that of pure PP. However, AS-BNC-2.5 has 207.244 MPa modulus, 32.092 MPa highest tensile strength, 29.120% tensile elongation, and 90.6950 Pa flexural strength, which was smaller than pure PP. The higher the degree of crystallinity of the antistatic bio-nano composites, the higher the tensile strength, but It's not for other mechanical properties of antistatic bio-nano composites. According to Shojaeiarani, Bajwa, and Chanda (2021), CNC has a large surface-to-volume ratio, high tensile strength (~10 GPa), high stiffness (~110–130 GPa), and high flexibility. Incorporating CNC in composites influenced their mechanical properties by improving filler-matrix compatibility and forming a filler network. Using CNC as a reinforcement agent improved the stress-transfer efficiency of the composites and the overall mechanical properties Shojaeiarani, Bajwa, and Chanda (2021).

Based on the results of the electrical resistivity of AS-BNC, the values were in the range of antistatic values of 10^{10} – 10^{12} Ω/sq. In addition, the surface resistivity value of AS-BNC was in the static dissipative value range of 10^{6} – 10^{12} Ω/sq, which has the potential to be used for electrostatic discharge prevention or the presence of a sudden electric current caused by an electric short circuit, a dielectric fault, or the contact between two electrically charged objects (Pang *et al.*, 2014). In general, the polymer matrix is highly insulated. Therefore, the presence of electrically conductive nanomaterials with a large aspect ratio dispersed in small quantities can drastically increase the electrical conductivity to a level that can support used for electrostatic discharge protection (Kumar *et al.*, 2019).

Table 4 Tensile properties of antistatic bio-nano composites

Treatments	Modulus (MPa)	Tensile strength (MPa)	Highest Strength (MPa)	Tensile elongation (%)	Break elongation (%)
Pure PP	**297.228 ± 5.90**	20.260 ± 1.96	**35.296 ± 0.52**	23.560 ± 0.22	553.506 ± 88.48
AS-BNC-0	217.952 ± 4.96	18.806 ± 2.63	33.846 ± 0.33	**25.608 ± 0.34**	**572.534 ± 332.56**
AS-BNC-0.5	236.768 ± 4.95	22.264 ± 6.15	35.178 ± 1.12	23.812 ± 2.62	173.532 ± 135.12
AS-BNC-2.5	207.244 ± 7.30	**30.376 ± 1.40**	32.092 ± 0.91	23.796 ± 1.71	29.120 ± 4.44

Table 5 Flexural, impact strength, and resistivity properties of antistatic bio-nano composites

Treatment	Modulus (MPa)	Strength (Pa)	Impact strength (J/m^2)	Resistivity (Ω/sq)
Pure PP	10.684 ± 0.00	90.706 ± 0.00	1.602 ± 0.00	10^{10-11}
AS-BNC-0	10.684 ± 0.00	90.706 ± 0.00	**1.996 ± 0.12**	10^{9-10}
AS-BNC-0.5	10.591 ± 0.00	**90.709 ± 0.00**	1.726 ± 0.21	10^{8-10}
AS-BNC-2.5	**11.071 ± 0.00**	90.695 ± 0.00	1.659 ± 0.32	**10^{10-12}**

Based on the results of mechanical properties, several test sub-parameters showed different tendencies compared to the results of the thermal properties test, except for yield strength and impact strength. This can occur due to uneven distribution of CNC particles in the PP matrix, excessive MAPP concentration, and preparation of the tensile test sample. It has been reported that using high concentrations of MAPP will provide many opportunities for the reinforcement material to bond to the polymer matrix. However, when MAPP completely covered the surface of the PP matrix, it did not produce better adhesion and decreased the mechanical properties of composites (Hassanabadi, Alemdar, and Rodrigue, 2015). Therefore, it was necessary to optimize the use of MAPP on CNC concentration.

The impact strength of AS-BNC decreased with increasing CNC concentration because the rigid nanoparticles increased the interfacial area between the matrix and fiber and

aided the possibility of crack initiation and propagation (Yousefian and Rodrigue, 2016; 2015). However, in the AS-BNC-2.5, the impact strength was still higher than Pure PP. This result indicated the presence of antistatic properties of M-DAG in line with resistivity analysis which was in the static dissipative range of 10^6 – 10^{12} Ω/sq (Pang *et al.*, 2014).

The yield strength of AS-BNC increased with increasing CNC concentration. According to Al-Haik *et al.* (2020), adding CNC to the PP matrix leads to a slight increase in yield strength (8%). However, the concentration of CNC above 2% indicated yield strength which tends to decrease to lower than Pure PP due to poor dispersion of CNC in the PP matrix and the weak chemical bonding between CNC and PP matrix.

The tensile modulus, highest tensile strength, break elongation, and flexural strength of AS-BNC showed a lower value than Pure PP, except for the break elongation of AS-BNC-0 and flexural strength of AS-BNC-0 and AS-BNC-0.5. Meanwhile, the flexural modulus of AS-BNC-2.5 showed a higher value than Pure PP. According to Adriana *et al.* (2014), a concentration of 1–5% CNC with the addition of 3% glycerol monostearate (GMS) as an antistatic agent on a polystyrene (PS) matrix showed the highest tensile modulus at 1 and 3% CNC (higher than Pure PS), while the tensile modulus was lower than Pure PS at concentrations of 2, 4, and 5% CNC, as well as at break elongation was lower than Pure PS for all treatments. In addition, Adriana *et al.* (2014) also reported that a concentration of 1–5% GSM with the addition of 3% CNC on the PS matrix showed the highest tensile modulus at 3% GMS (higher than Pure PS), while the tensile modulus was lower than Pure PS at concentrations of 1, 2, 4, and 5% GMS, as well as at break elongation was lower than Pure PS for all treatments, except for the addition of 1% GMS.

Using a CNC concentration of more than 2.5% can cause blockages in the molding machine. Therefore, the modification of the molding machine is required to minimize blockages during the antistatic bio-nano composites synthesis process. On the other hand, based on the color characteristics, antistatic bio-nano composites are difficult to color. Hence, the temperature control during the synthesis process needs to be optimized to minimize thermal degradation. The advantages are mono-diacylglycerols (M-DAG) can function as a lubricant so that the antistatic bio-nano composites synthesis process time is faster when compared to without the use of M-DAG, and can function as an inhibitor of thermal degradation during the synthesis of antistatic bio-nano composites.

4. Conclusions

Based on the results of SEM analysis on the cross-section, it was found that M-DAG and CNC agglomerations were found on the PP matrix. The XRD diffractogram pattern of AS-BNC showed peaks representing the diffraction structure of glycerol monostearate and cellulose I. It was observed that the particle size increased with an increase in CNC concentration in AS-BNC. The degree of crystallinity of AS-BNC-2.5 was higher than pure PP. The FTIR spectrum of each treatment was very similar to the characteristic peaks of PP and showed three distinct peaks of AS-BNC compared to pure PP. The melting temperature of AS-BNC-0 was 176.54 ^{0}C, which was higher than pure PP at 175.44 ^{0}C. The thermal stability of AS-BNC-0, AS-BNC-0.5, and AS-BNC-2.5 was 472.07 ^{0}C, 470.25 ^{0}C, and 475.15 ^{0}C, respectively, which was higher than that of pure PP at 468.27 ^{0}C. Furthermore, the MFI of AS-BNC-0 was lower than pure PP, while AS-BNC-0.5 and AS-BNC-2.5 had a higher MFI value than pure PP, with an increase of 32.0% and 43.9%, respectively. The mechanical properties results showed that the best formulation was AS-BNC-2.5 with 11.071 MPa flexural modulus, 30.376 MPa yield strength, 23.796% yield elongation, 1.659 J/m^2 impact strength, which was higher than pure PP, and antistatic at 10^{10} – 10^{12} Ω/sq resistivity. Further identification is needed to improve the characteristics of antistatic bio-nano

composites. Optimization of the conditions for the synthesis of antistatic bio-nano composites so that it does not easily cause clogging of the twin-screw extruder and injection molding machine and modification of the molding machine is needed to minimize the blockages during the synthesis of antistatic bio-nano composites.

Acknowledgments

Much appreciation goes to Palm Oil Plantation Fund Management Agency (POPFMA/BPDPKS) – Ministry of Finance RI for supporting this research trough Grant Research Sawit (GRS K18) No. PENG-1/DPKS.4/2018.

References

Adriana, Jalal, R., Thamrin, Wirjosentono, B., Gea, S., 2014. Mechanical Properties of Nanocrystal Cellulose Reinforced Polystyrene with Glycerol Monostearic as Antistatic Agent. *International Journal of ChemTech Research,* Volume 6(4), pp. 2421–2426

Al-Haik, M.Y., Aldajah, S., Siddique, W., Kabir, M.M., Haik, Y., 2020. Mechanical and Thermal Characterization of Polypropylene-reinforced Nanocrystalline Cellulose Nano-composites. *Journal of Thermoplastic Composite Materials,* Volume 20(10), pp. 1–12

Bhatnagar, N., Asija, N., 2016. Durability of High-performance Ballistic Composites. In: *Lightweight Ballistic Composites: Military and Law-Enforcement Applications,* Bhatnagar, A. (Eds.), Woodhead Publishing, Inc. Sawston, Cambridge, United Kingdom, pp. 231–283

Brinkmann, A., Chen, M., Couillard, M., Jakubek, Z.J., Leng, T., Johnston, L.J., 2016. Correlating Cellulose Nanocrystal Particle Size and Surface Area. *Langmuir*, Volume 32(24), pp. 6105−6114

Chakraborty, B.C., Ratna, D., 2020. Experimental Techniques and Instruments for Vibration Damping. In: *Polymers for Vibration Damping Applications,* Chakraborty, B.C., Ratna, D. (Eds.), Elsevier Inc., Amsterdam, The Netherlands, pp. 281–325

Clemons, C., Rick, R., 2020. Preparation of Cellulose Nanocrystal-polyoropylene Masterbatches by Water-assisted Thermokinetic Mixing. *In:* ANTEC 2020: The Virtual Edition, pp. 1–6

Couret, L., Irle, M., Belloncle, C., Cathala, B., 2017. Extraction and Characterization of Cellulose Nanocrystals from Post-consumer Wood Fiberboard Waste. *Cellulose,* Volume 24(5), pp. 1–13

Fang, J., Zhang, L., Sutton, D., Wang, X., Lin, T., 2012. Needleless Melt-electrospinning of Polypropylene Nanofibres. *Journal of Nanomaterials,* Volume 2012, pp. 1–9

Guerra, V., Wan, C., McNally, T., 2019. Nucleation of the β-polymorph in Composites of Poly(Propylene) and Graphene Nanoplatelets*. Journal of Composites Science,* Volume 3(38), pp. 1–11

Gwon, J.G., Cho, H.J., Lee, D., Choi, D.H., Lee, S., Wu, Q., Lee, S.Y., 2018. Physicochemical and Mechanical Properties of Polypropylene-cellulose Nanocrystal Nanocomposites: Effects of Manufacturing Process and Chemical Grafting*. BioResources,* Volume 13(1), pp. 1619–1636

Hassanabadi, H.M., Alemdar, A., Rodrigue, D., 2015. Polypropylene Reinforced with Nanocrystalline Cellulose: Coupling Agent Optimization*. Journal of Applied Polymer Science,* Volume 132(34), p. 42438

Hejna, A., Kirpluks, M., Kosmela, P., Cabulis, U., Haponiuk, J., Piszczyk, Ł., 2017. The Influence of Crude Glycerol and Castor Oil-based Polyol on the Structure and Performance of

Rigid Polyurethane-polyisocyanurate Foams. *Industrial Crops and Products,* Volume 95(1), pp. 113–125

Hobuss, C.B., Da Silva, F.A., Dos Santos, M.A.Z., De Pereira, C.M.P., Schulz, G.A.S., Bianchini, D., 2020. Synthesis and Characterization of Monoacylglycerols through Glycerolysis of Ethyl Esters Derived from Linseed Oil by Green Processes*. RSC Advances,* Volume 10, pp. 2327–2336

Jain, R., Tiwari, A., 2015. Biosynthesis of Planet Friendly Bioplastics using Renewable Carbon Source. *Journal of Environmental Health Science and Engineering,* Volume 13(11), pp. 1–5

Kafy, A., Kim, H.C., Zhai, L., Kim, J.W., Hai, L. Van, Kang, T.J., Kim, J., 2017. Cellulose Long Fibers Fabricated from Cellulose Nanofibers and Its Strong and Tough Characteristics. *Scientific Reports,* Volume 7, p. 17683

Kumar, P., Narayan Maiti, U., Sikdar, A., Kumar Das, T., Kumar, A., Sudarsan, V., 2019. Recent Advances in Polymer and Polymer Composites for Electromagnetic Interference Shielding: Review and Future Prospects. *Polymer Reviews,* Volume 59(4), pp. 687–738

Maryniak, W.A., Uehara, T., Noras, M.A., 2003. Surface Resistivity and Surface Resistance Measurements. *Trek Application Note,* Volume 2003(1005), pp. 195–209

McKeen, L.W., 2014. Introduction to Plastics, Polymers, and Their Properties. In: *The Effect of Temperature and other Factors on Plastics and Elastomers,* McKeen, L.W. (Eds.), William Andrew, Inc. Norwich, New York, pp. 1–45

Moser, C., Henriksson, G., Lindström, M.E., 2016. Specific Surface Area Increase During Cellulose Nanofiber Manufacturing Related to Energy Input. *BioResources,* Volume 11(3), pp. 7124–7132

Ng, H.M., Sin, L.T., Bee, S.T., Tee, T.T., Rahmat, A.R., 2017. Review of Nanocellulose Polymer Composite Characteristics and Challenges. *Polymer – Plastics Technology and Engineering,* Volume 56(7), pp. 687–731

Pang, H., Xu, L., Yan, D.X., Li, Z.M., 2014. Conductive Polymer Composites with Segregated Structures. *Progress in Polymer Science,* Volume 39(11), pp. 1908–1933

Park, S., Baker, J.O., Himmel, M.E., Parilla, P.A., Johnson, D.K., 2010. Cellulose Crystallinity Index: Measurement Techniques and Their Impact on Interpreting Cellulase Performance. *Biotechnology for Biofuels,* Volume 3(1), pp. 1–10

Purnomo, H., Baskoro, H., Muslim, F., 2021. Stress and Strain Behavior of Confined Lightweight Concrete using Sand Coated Polypropylene Coarse Aggregate. *International Journal of Technology,* Volume 12(6), pp. 1261–1272

Rahman, N.A., Hassan, A., Heidarian, J., 2018. Effect of Compatibiliser on the Properties of Polypropylene/Glass Fibre/Nanoclay Composites. *Polimeros,* Volume 28(2), pp. 1–9

Rochardjo, H.S.B., Fatkhurrohman, Kusumaatmaja, A., Yudhanto, F., 2021. Fabrication of Nanofiltration Membrane based on Polyvinyl Alcohol Nanofibers Reinforced with Cellulose Nanocrystal using Electrospinning Techniques. *International Journal of Technology,* Volume 12(2), pp. 329–338

Sabaruddin, F.A., Md-Tahir, P., Lee, S.H., 2019. Mechanical Properties of PP/Kenaf Core Nanocomposites Made from Nanocrystalline Cellulose as An Additive. *Journal of Reinforced Plastics and Composites,* Volume 38(2), pp. 88–95

Saleh, T.A., 2021. Structural Characterization of Hybrid Materials. In: *Polymer Hybrid Materials and Nanocomposites*, Saleh, T.A. (Eds.), William Andrew, Inc. Norwich, New York, pp. 213-240

Salsabila, S., Setyaningsih, D., Jannah, Q.R., Muna, N., 2021. Formulation of Mono-diacylglycerol from Palm Fatty Acid Distillate and Glycerol as Antistatic Agents on

Plastics. *In:* IOP Conference Series: Earth and Environmental Science, Volume 749, p. 012069

Sandri, G., Bonferoni, M.C., Rossi, S., Ferrari, F., Aguzzi, C., Viseras, C., Caramella, C., 2016. Clay Minerals for Tissue Regeneration, Repair, and Engineering. *In:* Wound Healing Biomaterials, Ågren, M.S. (Eds.), Woodhead Publishing, Inc. Sawston, Cambridge, United Kingdom, pp. 385–402

Sarfat, M.S., Setyaningsih, D., Fahma, F., Indrasti, N.S., Sudirman, 2022. Characterization of Mono-diacylglycerols, Cellulose Nanocrystals, Polypropylene, and Supporting Materials as raw Materials for Synthesis of Antistatic Bionanocomposites. *In:* IOP Conference Series: Earth and Environmental Science, Volume 1034, pp. 012009

Setyaningsih, D., Suwarna, M.A., Muna, N., 2020. The effect of Solvent Type and Temperature on Mono-diacylglycerol Purification. *In:* IOP Conference Series: Earth and Environmental Science, Volume 460, p. 012037

Setyaningsih, D., Warsiki, E., Ulfa, S.F., Muna, N., 2020b. The Effect of Sodium Carbonate and Saccharides on Mono-diacylglycerol (M-DAG) Purification. In: IOP Conference Series: Earth and Environmental Science, Volume 460, pp. 012038

Shieddieque, A.D., Mardiyati, Suratman, R., Widyanto, B., 2021. Preparation and Characterization of Sansevieria Trifasciata Fiber/High-Impact Polypropylene and Sansevieria Trifasciata Fiber/Vinyl Ester Biocomposites for Automotive Applications. *International Journal of Technology,* Volume 12(3), pp. 549–560

Shojaeiarani, J., Bajwa, D.S., Chanda, S., 2021. Cellulose Nanocrystal Based Composites: A Review. *Composites Part C: Open Access,* Volume 5, p. 100164

Shubhra, Q.T.H., Alam, A.K.M.M., Quaiyyum, M.A., 2013. Mechanical Properties of Polypropylene Composites: A Review. *Journal of Thermoplastic Composite Materials*, Volume 26, pp. 362–391

Tang, J., Sisler, J., Grishkewich, N., Tam, K.C., 2017. Functionalization of Cellulose Nanocrystals for Advanced Applications. *Journal of Colloid and Interface Science,* Volume 494, pp. 397–409

Thomas, B., Raj, M.C., Athira, B.K., Rubiyah, H.M., Joy, J., Moores, A., Drisko, G.L., Sanchez, C., 2018. Nanocellulose, a Versatile Green Platform: From Biosources to Materials and Their Applications. *Chemical Reviews,* Volume 118(24), pp. 11575–11625

Yousefian, H., Rodrigue, D., 2015. Nano-crystalline Cellulose, Chemical Blowing Agent, and Mold Temperature Effect on Morphological, Physical/Mechanical Properties of Polypropylene. *Journal of Applied Polymer Science,* Volume 132(47), pp. 428–445

Yousefian, H., Rodrigue, D., 2016. Effect of Nanocrystalline Cellulose on Morphological, Thermal, and Mechanical Properties of Nylon 6 Composites. *Polymer Composites,* Volume 37, pp. 1473–1479

Yusuf, M., Khan, M., Khan, R.A., Ahmed, B., 2013. Preparation, Characterization, In Vivo and Biochemical Evaluation of Brain Targeted Piperine Solid Lipid Nanoparticles in an Experimentally Induced Alzheimer's Disease Model. *Journal of Drug Targeting,* Volume 21(3), pp. 300–311

Zhou, X., Yu, Y., Lin, Q., Chen, L., 2013. Effects of Maleic Anhydride-grafted Polypropylene (MAPP) on the Physico-mechanical Properties and Rheological Behavior of Bamboo Powder-polypropylene Foamed Composites. *BioResources,* Volume 8(4), pp. 6263–6279